Anisotropic, Organic Ionic Plastic Crystal Mesophases from Persubstituted Imidazolium Pentacyanocyclopentadienide Salts

Karel Goossens, Lena Rakers, Benoît Heinrich, Guillermo Ahumada, Takahiro Ichikawa, Bertrand Donnio, Tae Joo Shin, Christopher Bielawski, Frank Glorius

Anisotropic, Organic Ionic Plastic Crystal Mesophases from Persubstituted Imidazolium Pentacyanocyclopentadienide Salts

Karel Goossens*, Lena Rakers, Benoît Heinrich, Guillermo Ahumada, Takahiro Ichikawa, Bertrand Donnio, Tae Joo Shin, Christopher W. Bielawski*, Frank Glorius*

Cite this: *Chem. Mater.* 2019, 31, 9593–9603
Publication Date:November 26, 2019
https://doi-org.scd-rproxy.u-strasbg.fr/10.1021/acs.chemmater.9b02338

Abstract We describe the synthesis, supramolecular organization, and thermal characteristics of an unprecedented family of symmetric 1,2,3,4,5-pentaalkylimidazolium ($[(C_n)_5im]^+$) salts equipped with halide, nitrate, or pentacyanocyclopentadienide ($[Cp(CN)_5]^-$) counterions. Salts containing relatively small anions were obtained as low-melting solids, whereas those with $[Cp(CN)_5]^-$ anions were found to be ionic liquids even below room temperature. A permethylated derivative, $[(C_1)_5im][Cp(CN)_5]$, proved to be exceptional. Upon heating, the salt self-organized into a new type of organic ionic plastic crystal (OIPC) mesophase, which was termed M_{hex} and whose anisotropic structure featured hexagonally ordered, rotating anionic stacks positioned within a continuum composed of disordered cations. The structure of the mesophase resembles that of classical columnar liquid-crystalline phases, despite the absence of long, flexible chains. In the M_{hex} phase, the cations surrounding the anionic columns effectively fulfill the role of "softening" structural constituents, much in the same way as flexible chains. The discovery of the novel mesophase, which displays a two-dimensional, and thus intrinsically anisotropic, lattice resulting from the rotation of entire ionic assemblies around a columnar axis, represents a new paradigm in the field of OIPCs. Relatively high ionic conductivities were measured in the M_{hex} phase, particularly after doping with the corresponding sodium salt, $Na[Cp(CN)_5]$, demonstrating the materials' potential for use in electrochemical applications such as sodium-ion batteries.

1. Introduction

A wide variety of organic cations have been used to obtain ionic liquids (ILs) as "designer" solvents(1-3) as well as to synthesize ionic liquid crystals (ILCs) expected to show anisotropic physical properties.(4−7) Besides other applications, both classes of materials have attracted widespread interest for their potential use as nonvolatile electrolytes in various electrochemical devices, such as lithium-ion or sodium-ion batteries, fuel cells, and dye-sensitized solar cells.(8−15)

1,3-Disubstituted imidazoliums are emblematic cations which are among the most frequently selected partners for incorporation into ILs and ILCs.(16−19) The nature of the imidazolium substituents as well

as the type of the anion selected can strongly impact the physical properties of the corresponding salts, including their melting and clearing temperatures, decomposition temperature, viscosity, and ionic conductivity. For example, fluorinated anions are known to increase thermal stability and reduce viscosity.(20) Likewise, halogen-free, cyano-substituted anions, such as $[N(CN)_2]^-$ and $[C(CN)_3]^-$, have been reported to yield ILs that feature low viscosities and high ionic conductivities.(21,22) Moreover, some of us recently reported a series of $[N(CN)_2]^-$ salts that self-organized into liquid-crystalline (LC) mesophases.(23)

Although LC phases are often observed upon the attachment of long alkyl or fluoroalkyl chains, or mesogenic groups, to cationic species,(4,5) the use of relatively short substituents commonly results in nonmesomorphic ILs or, in some cases, salts that adopt organic ionic plastic crystal (OIPC) phases. OIPCs constitute an emerging field of materials science and are intensively investigated as "solid" electrolytes for use in applications that require high ionic conductivities.(24−30) The plasticity of OIPC mesophases and their ability to flow under mechanical stress stem from structural disorder due to rotational or reorientational short-range motions of the cationic and/or anionic species that are otherwise part of a long-range correlated lattice.(31) The short-range dynamic disorder leads to enhanced translational motion for individual ions as well as to lattice vacancies.(32) Whereas *N*-alkyl-*N*-methylpyrrolidinium cations have been extensively used to obtain OIPC phases, examples of imidazolium-based plastic crystals are scarce.(33−39) MacFarlane and co-workers attributed the lower tendency of imidazolium salts to adopt OIPC phases to charge delocalization which ultimately weakens interionic interactions.(40) Consequently, short-chain-substituted imidazolium salts often melt to a liquid state before a stable plastic crystal phase is formed.

In search of new ionic compounds and molecular architectures that adopt LC or OIPC phases, or that behave as ILs at reasonably low temperatures, we considered salts with 1,2,3,4,5-pentaalkyl-1*H*-imidazol-3-ium ($[(C_n)_5im]^+$) cations. Although the influence of installing alkyl or aryl substituents in the 2-positions of imidazoliums on the thermal characteristics of the corresponding ILs and ILCs has been explored,(41−47) peralkylated derivatives (i.e., $[(C_n)_5im][X]$ with $n \geq 2$) have not yet been reported in detail.(48,49) Persubstitution was envisioned to result in a protective hydrophobic shell around the cationic heterocycle and to facilitate long-range molecular ordering, particularly in combination with planar counterions. Recently, some of us prepared 4,5-dialkylsubstituted imidazoles with relatively long alkyl substituents by utilizing Radziszewski-type chemistry as a key step. The corresponding 1,3-dimethylimidazolium salts were obtained upon methylation and applied as lipid analogues in model cell systems or used as precursors for *N*-heterocyclic carbenes for the stabilization of nanoparticles.(50−54) We also reported 1,2,3-trimethyl-4,5-bis(*n*-pentadecyl)imidazolium iodide to be the first example of a LC pentasubstituted imidazolium salt.(55)

We describe here how the previously reported synthetic methodology may be extended to obtain $[(C_n)_5im][X]$ salts that feature alkyl substituents larger than a methyl group (i.e., *n*-C_7H_{15}, *n*-$C_{11}H_{23}$ or *n*-$C_{15}H_{31}$). Derivatives with planar nitrate ($[NO_3]^-$) or "π-electronic" pentacyanocyclopentadienide ($[Cp(CN)_5]^-$) anions (Scheme 1) were subsequently prepared from the halide salts by anion metathesis. The thermal characteristics of the aforementioned compounds as well as those of permethylated homologues were also examined. During the course of these studies, it was discovered that $[(C_1)_5im][Cp(CN)_5]$ adopted an unprecedented, anisotropic OIPC mesophase and was found to exhibit high ionic conductivity values, especially after doping with a Na^+ salt. $[Cp(CN)_5]^-$ was identified as a stable and compact mesogenic building block that maintains a "charge-segregated" stacking, even at elevated temperatures. The following discussions and implications of the findings will be focused accordingly.

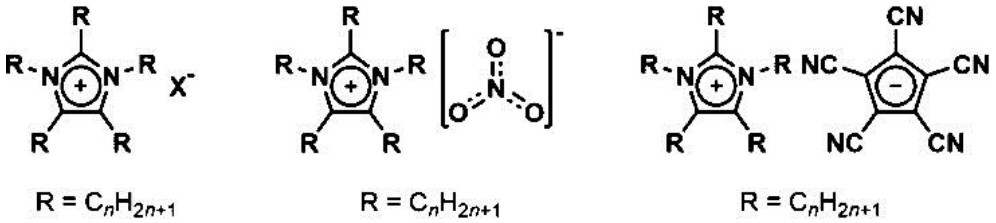

Scheme 1. Examples of 1,2,3,4,5-Pentaalkyl-1*H*-imidazol-3-ium Salts with Halide (X^- = Br^- and I^-), $[NO_3]^-$, or $[Cp(CN)_5]^-$ Anions

2. Results and Discussion

2.1. Synthesis of Pentaalkylimidazolium Salts As shown in Scheme 2, condensing commercially available aldehydes $C_nH_{2n+1}CHO$ **1-*n*** with 1,2-diketones **3-*n***(51) in the presence of NH_4OAc afforded the corresponding 2,4,5-trialkyl-1*H*-imidazoles **4-*n***. Subsequent *N*-alkylation using an excess of $C_nH_{2n+1}Br$ (*n* = 7, 11, and 15) yielded the desired $[(C_n)_5im][Br]$ salts (**5-Br-*n***).(56) In parallel, the $[(C_1)_5im]^+$ salt **5-I-1** was also prepared from 1,2,4,5-tetramethyl-1*H*-imidazole and CH_3I under Menschutkin-type conditions. To understand how the nature of the anion influenced the thermal characteristics of the corresponding salts, anion exchange for $[NO_3]^-$ or $[Cp(CN)_5]^-$ counterions was accomplished by treating the halide salts with $AgNO_3$ or $Na[Cp(CN)_5]$, which was prepared from NaCN and CS_2 (see Scheme S1).(57) Based on combustion elemental analysis data, all of the halide salts as well as **5-Cp(CN)$_5$-1** and **5-Cp(CN)$_5$-15** were obtained as quasi-anhydrous compounds, whereas the other $[Cp(CN)_5]^-$ salts and the $[NO_3]^-$ salts were obtained as hemihydrates.(58)

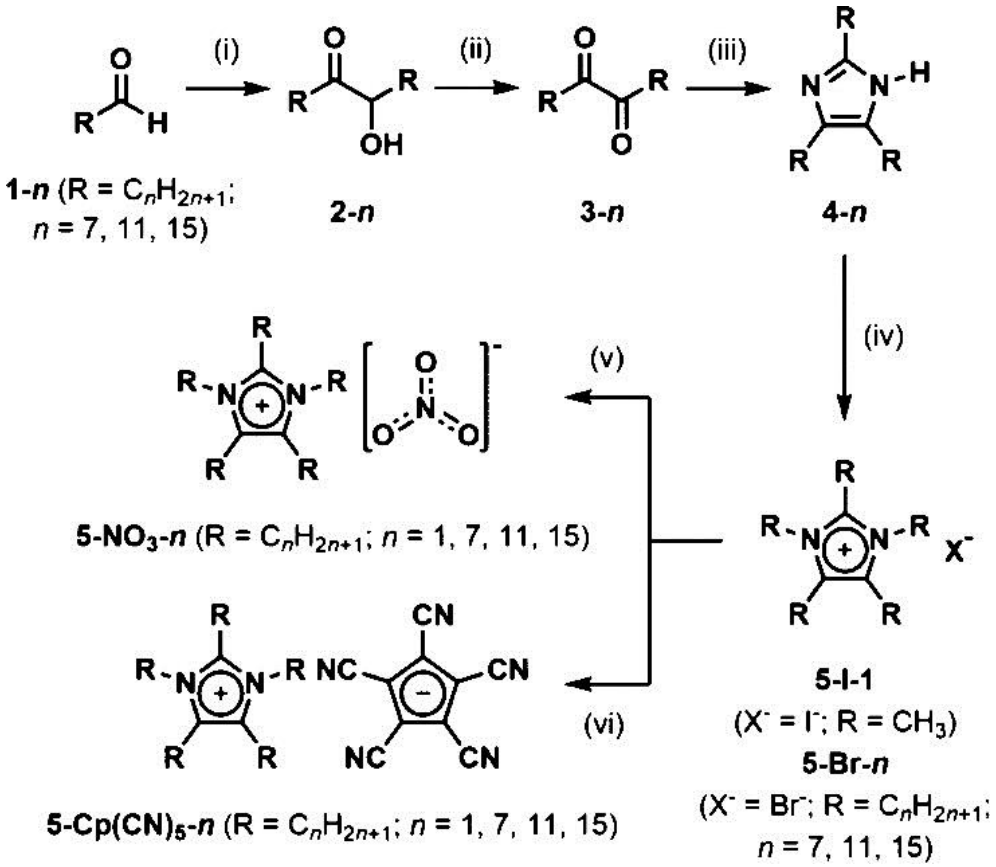

Scheme 2. Synthesis of the Pentaalkylimidazolium Salts $[(C_n)_5im][X]$ (**5-X-*n***) Reagents and conditions: (i) NEt_3, 3-benzyl-5-(2-hydroxyethyl)-4-methylthiazol-3-ium chloride, EtOH, reflux, and Ar (3 h); (ii) $VOCl_3$, O_2, CH_3CN, and r.t. (18 h); (iii) **1-*n***, NH_4OAc, HOAc, EtOH, 110 °C, and Ar (18 h) (yields: **4-7**: 60%, **4-11**: 69%, and **4-15**: 29%); (iv) (1) $C_nH_{2n+1}Br$ (15 equiv), K_2CO_3, THF, 80 °C, and Ar (3 days); (2) an isolated mixture of **5-Br-*n*** and the 1,2,4,5-tetraalkylimidazole byproduct: $C_nH_{2n+1}Br$ (15 equiv), K_2CO_3, THF, 80 °C, and Ar (3 days) (yields for (1) + (2): **5-Br-7**: 28 + 49%, **5-Br-11**: 27 + 32%, and **5-Br-15**: 52%) [remark: **5-I-1** was prepared from 1,2,4,5-tetramethyl-1*H*-imidazole in 95% yield]; (v) $AgNO_3$ (1.0 equiv), H_2O, and r.t. (1.5 h) (for **5-NO_3-1**) or $AgNO_3$ (1.1 equiv), EtOH, and r.t. (15 h) (for **5-NO_3-*n*** (*n* = 7, 11, and 15)) (yields: **5-NO_3-1**: 95%, **5-NO_3-7**: 78%, **5-NO_3-11**: 80%, and **5-NO_3-15**: 73%); and (vi) $Na[Cp(CN)_5]$(57) (0.9 equiv), H_2O, and r.t. (1 h) (for **5-Cp(CN)$_5$-1**) or $Na[Cp(CN)_5]$(57) (1.0 equiv), CH_3CN, and r.t. (1 h) (for **5-Cp(CN)$_5$-*n*** (*n* = 7 and 11)) or 65–70 °C (1 h) (for **5-Cp(CN)$_5$-15**) (yields: **5-Cp(CN)$_5$-1**: 77%, **5-Cp(CN)$_5$-7**: 99%, **5-Cp(CN)$_5$-11**: 98%, and **5-Cp(CN)$_5$-15**: 99%).

2.2. Thermal Characteristics and Structural Elucidation of Crystal and Plastic Crystal Phases The thermal characteristics of the synthesized pentaalkylimidazolium salts were examined using thermogravimetric analysis (TGA), differential scanning calorimetry (DSC), and polarized-light optical microscopy (POM). The key results are summarized in Table 1 (see also Figures S8–S23). The decomposition temperatures of $[(C_1)_5im][X]$ salts were measured to be significantly higher than those of the homologues with longer alkyl chains and decreased in the following order: $[Cp(CN)_5]^- > [NO_3]^- > I^-$. None of the amphiphilic salts **5-X-*n*** (X^- = Br^-, $[NO_3]^-$, and $[Cp(CN)_5]^-$; *n* = 7, 11, and 15) were found to adopt LC mesophases. The compounds melted directly to isotropic liquids without passing through intermediate LC phases and, in the case of $[Cp(CN)_5]^-$ salts, were found to be viscous liquids at ambient temperature. Likewise, variable temperature, small- to wide-angle X-ray scattering (SWAXS) measurements on powder samples of **5-X-*n*** (X^- = Br^-, $[NO_3]^-$; *n* = 11 and 15) revealed that the pristine samples were solids of low crystallinity and that cooling from the melts yielded even lower crystallinities because of slow crystallization kinetics (Figures S36–S39). We refer to Section S8 in the Supporting Information for a comparison with the thermal characteristics of long-chain-substituted 1-alkyl-3-methylimidazolium ($[C_nmim]^+$) and 1,3-dialkylimidazolium ($[(C_n)_2im]^+$) salts and for an in-depth discussion of the effect of symmetric pentasubstitution on the mesomorphic properties of imidazolium salts. The salts **5-I-1** and **5-NO_3-1** also did not exhibit mesophases based on POM and DSC observations.

Significantly different results were obtained upon analysis of **5-Cp(CN)$_5$-1**. DSC measurements revealed two pronounced thermal events during heating and cooling of the salt (Figure S16) apart from a small enthalpy change due to a crystal-to-crystal transition ($Cr_1 \rightarrow Cr_2$, see Table S2). POM studies revealed that **5-Cp(CN)$_5$-1** melts to a plastic, birefringent, enantiotropic mesophase at ∼234 °C before clearing to an isotropic liquid at ∼240 °C. The observed textures indicated that a columnar type of mesophase formed with a pronounced tendency toward homeotropic alignment (Figures 1 and S1–S5).

Table 1. Phase Transition Temperatures and Thermal Data Recorded for the Pentaalkylimidazolium Salts 5-X-*n*[a]

compound	transition[b]	*T* (°C)[c]	Δ*H* (kJ mol^{-1})[d]	Δ*S* (J K^{-1} mol^{-1})[e]	$T_{1\%}$ (°C)[f]
5-I-1	Cr → Iso	214[g]	22.7	~47	~231
5-Br-7	S → Iso[a]	46[g]	1.8	~6	~188
5-Br-11	S → Iso[a]	40, 54, 59[a]	42.0a	[h]	~183
5-Br-15	S → Iso[a]	78, 81a	82.8[a]	[h]	~193
5-NO_3-1	Cr → Iso	154[g]	13.2	~31	~267
5-NO_3-7	S_1 + Iso → S_2[a]	–8[g]	–12.3	~–46	~175
	S_2 → S_1 + Iso[a]	19[g]	11.4	~39	
	S_1 + Iso → Iso[a]	45	1.1	3	
5-NO_3-11	S → Iso	52[g]	33.1	~102	~185
5-NO_3-15	S → Iso	72[g]	77.6	~225	~204
5-$Cp(CN)_5$-1	Cr → M_{hex}	234	16.4	32	~369
	M_{hex} → Iso	240	11.9	23	
5-$Cp(CN)_5$-7	g → Iso	14	-	-	~192
5-$Cp(CN)_5$-11	S → Iso	–6	9.7	36	~175
5-$Cp(CN)_5$-15	S → Iso	16	92.9	321	~221

[a]See Table S2 for additional data and information. [b]Abbreviations: Cr = crystalline phase; g = glass; S, S_1, and S_2 = solid phase(s) (not or only partially crystalline); M_{hex} = plastic crystal mesophase with 2D hexagonal symmetry; and Iso = isotropic liquid phase. [c]Onset temperatures obtained by DSC during the second heating run at a rate of 10 °C min^{-1} and under an atmosphere of N_2. A small hole was pierced into the lid of the DSC sample pans. [d] Enthalpy change. [e] Entropy change. [f]Temperature at which 1% weight loss was measured by TGA at a rate of 5 °C min^{-1} and under an atmosphere of N_2 (neglecting initial small weight losses attributed to the release of H_2O). [g]Peak temperature. [h]An accurate value forthe entropy of fusion, ΔS_{fus}, could not be obtained because of the overlap between transitions.

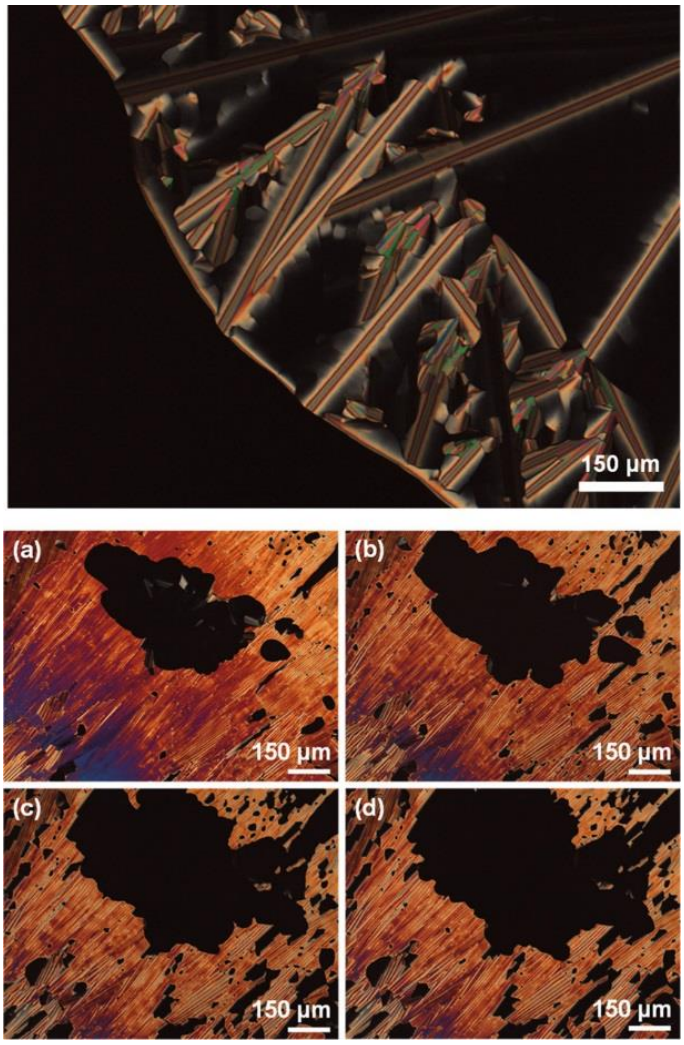

Figure 1. POM images of the M_{hex} phase of **5-Cp(CN)$_5$-1** at 239 °C. (Bottom) (a) Picture taken immediately after pressing the sample with a needle. (b–d) Pictures showing the further evolution of the texture over the course of 40 s during which time no pressure was applied to the sample [the same sample area is shown in images (a–d)]. All images were recorded using crossed polarizers.

To gain additional insight into the structure adopted by **5-Cp(CN)$_5$-1** in the Cr_1 phase, single-crystal X-ray diffraction (XRD) data were collected at −150 °C. Although an alternating packing(59) of the cations and anions, which are complementary in size and shape, may be expected, the solid-state structure of **5-Cp(CN)$_5$-1** features stacks of tilted $[Cp(CN)_5]^-$ anions in the direction of the *a*-axis that are laterally separated by $[(C_1)_5im]^+$ cations whose ring planes are oriented parallel to the columnar axes (Figures 2 and S28–S31). The packing is stabilized by intermolecular C–H···N hydrogen bonds between the methyl groups of the cations and the cyano nitrogen atoms of the anions (Table S5).

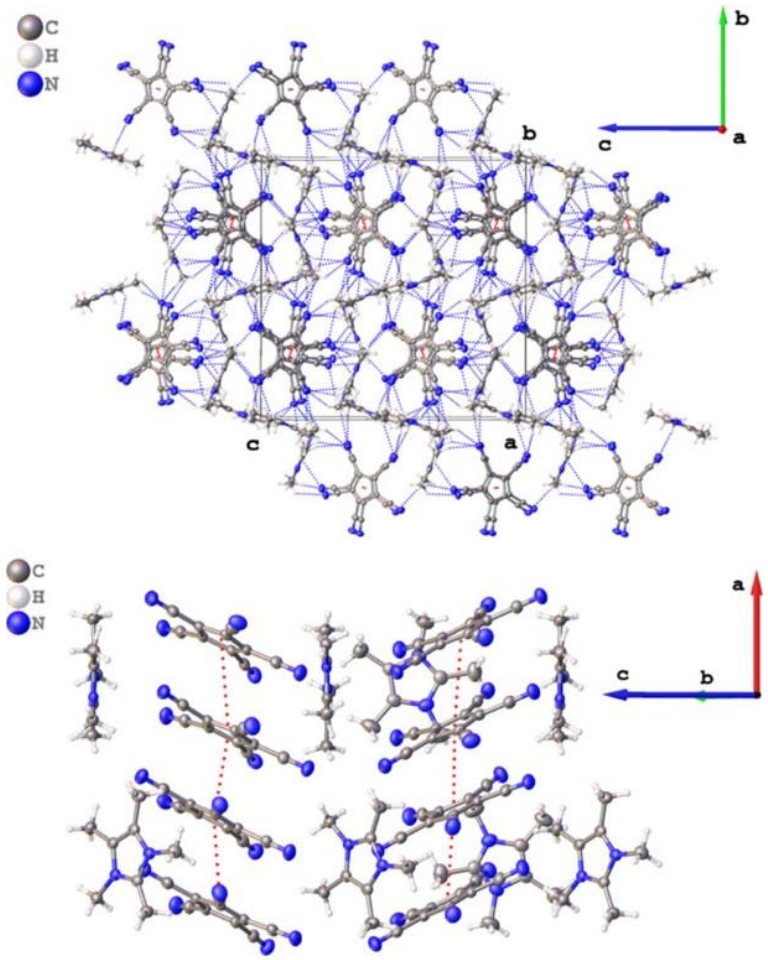

Figure 2. (Top) Packing in the crystal structure of **5-Cp(CN)$_5$-1**, showing the columnar stacking of the $[Cp(CN)_5]^-$ anions and the linkage of the molecules through nonclassical C–H···N hydrogen bonds (blue dotted lines). (Bottom) View along the *b*-axis, showing the ring-to-ring interactions between $[Cp(CN)_5]^-$ anions (red dotted lines). See also Section S6.2 in the Supporting Information.

The single-crystal XRD results for the Cr_1 phase of **5-Cp(CN)$_5$-1** were used to derive the orthorhombic unit cell parameters of its Cr_2 phase from the SWAXS powder pattern that was recorded at 200 °C (Figure S33 and Table S7). The cross-sectional area S_{col} of one column of stacked $[Cp(CN)_5]^-$ anions along the *a*-axis surrounded by $[(C_1)_5im]^+$ cations in the Cr_2 phase was calculated as $(b \times c)/4 = 126.6$ Å^2. The thickness of one columnar slice was estimated as $h_{mol} = V_{mol}/S_{col} = a/4 = 3.94$ Å (where V_{mol} is the molecular volume). The results were then compared to the geometric parameters of the thermotropic mesophase that were derived from synchrotron-based SWAXS measurements at 240 °C. In addition to several broad scattering signals, the SWAXS pattern contained four sharp reflections characterized by an inverse *d*-spacing ratio of 1:√3:2:√7 (Figure 3 and Table S8). The signals were indexed as the (10), (11), (20), and (21) reflections of a two-dimensional (2D) hexagonal lattice with a lattice parameter $a_{hex} \approx 12.31$ Å; hence, the columnar mesophase was designated as M_{hex}. The 2D lattice area S_{col} corresponded to $(\sqrt{3}/2)a_{hex}^2 \approx 131.2$ Å^2 and h_{mol} to $V_{mol}/S_{col} = 4.1(\pm0.2)$ Å (V_{mol} was estimated to be 536(±20) Å^3 from reference dilatometric data).

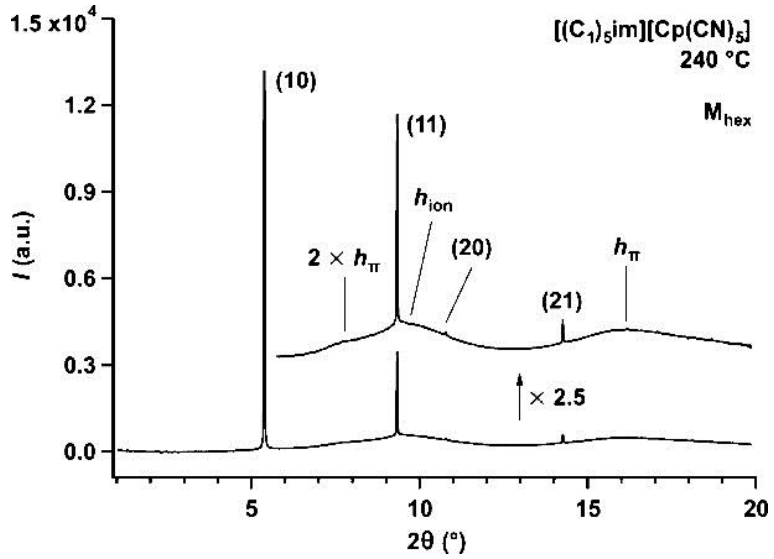

Figure 3. Synchrotron-based SWAXS pattern that was recorded for the M_{hex} mesophase of **5-Cp(CN)$_5$-1** at 240 °C (the X-ray wavelength used was 1.00 Å). See also Table S8 in the Supporting Information.

The geometric parameters described above indicated that the local molecular arrangements in the crystal phases and the mesophase are similar, with the differences attributable to thermal expansion (see also Section S6.2 in the Supporting Information). In the mesophase, the $[Cp(CN)_5]^-$ anions are π-stacked into columns, albeit in an irregular manner as evidenced by the broad h_π scattering signal centered at ∼3.6 Å (Figure 3). Heating above the melting point also reduces the correlation between the respective, tilt-induced (c.f., $h_{mol} > h_\pi$) orientations of the $[Cp(CN)_5]^-$ stacks and the relative positions of the surrounding $[(C_1)_5im]^+$ cations. This process is accompanied by the onset of rotation of the $[Cp(CN)_5]^-$ stacks. The disorder causes the formation of columns with an average cylindrical shape and facilitates merging of the peripheral cations to form a continuum (Figure 4). The broad scattering signal h_{ion}, centered at ∼5.9 Å (Figure 3), arises from the average, close-packed distances between the $[(C_1)_5im]^+$ cations that have lost long-range positional order. The resulting time- and space-averaged hexagonal symmetry and organization, as observed by SWAXS, is similar to that of hexagonal columnar LC mesophases (Col_{hex}) adopted by classical discotic mesogens that consist of planar aromatic cores with peripheral alkyl chains, in which case the molten alkyl chains form a continuum.(60)

Despite the structural similarity to Col_{hex} phases, the mesophase adopted by **5-Cp(CN)$_5$-1** is not a liquid crystal phase that involves molten chains but rather an ionic plastic crystal (OIPC) phase for which the mesomorphism originates from dynamic disorder. Indeed, **5-Cp(CN)$_5$-1** solely consists of cations and anions that lack flexible chains and have a defined conformation because of their rigid structure (except for the ability of the methyl groups in the $[(C_1)_5im]^+$ cations to rotate about their C–C or C–N bond axes(61)). In OIPC phases, the individual cations and/or anions typically rotate around the lattice points of a three-dimensional (3D) lattice, leading to an isotropic or weakly anisotropic arrangement of quasi-globular objects. In contrast, the OIPC phase of **5-Cp(CN)$_5$-1** features a 2D, and thus intrinsically anisotropic, lattice resulting from the rotation of entire ionic assemblies around a columnar axis. The molecular arrangements in the crystalline solid phases, featuring approximately cylindrical assemblies of stacked anions "wrapped" by cations, prefigure the aforementioned motions in the OIPC phase. We note that **5-Cp(CN)$_5$-1** is among the few examples of halogen-free OIPC materials that are known to date, complementing, for instance, more archetypical $[N(CN)_2]^-$,(21,62−64) $[SCN]^-$,(65,66) $[CH_3SO_3]^-$,(37,67) and $[H_2PO_4]^-$(36,68) salts.

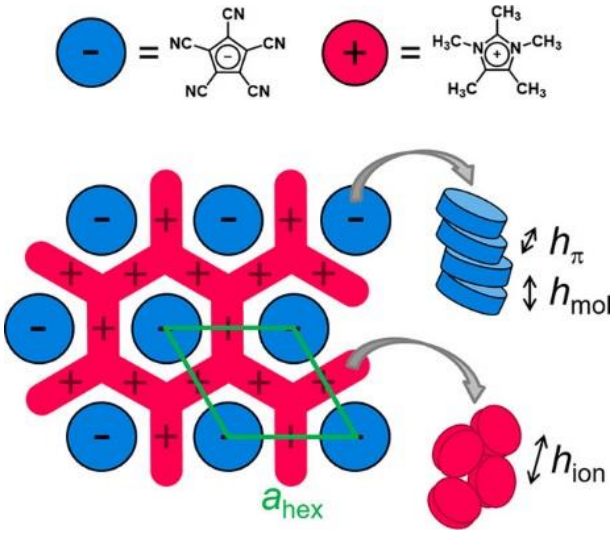

Figure 4. Schematic view of the supramolecular packing in the M_{hex} mesophase of **5-Cp(CN)$_5$-1**. The 2D unit cell parameter is indicated by a_{hex}. The phase features rotating columnar stacks of $[Cp(CN)_5]^-$ anions that are arranged in a hexagonal lattice and positioned within a continuum formed by molten $[(C_1)_5im]^+$ cations that play the role of disorderly components. In classical LC Col_{hex} mesophases, such a continuum is composed of molten chains.

Although the structure of the M_{hex} OIPC phase is, to the best of our knowledge, unprecedented, comparison to nonionic systems may be valuable. For instance, the so-called "rotator phases" that are adopted by long-chain *n*-alkanes in certain temperature ranges in which they are still mainly in their "stiff", all-trans conformations also consist of units that rotate about parallel axes, which, in those cases, correspond to the chain backbones.(69) In the columnar mesophases that were reported by Ros and co-workers, the rotating units are columns of π-stacked indene- and pseudoazulene-based aromatic cores that are arranged in a 2D hexagonal sublattice.(70,71) The molecules did not contain peripheral chains but featured polarizable atoms (halogens, S) and/or polar groups (−C≡N, >C═O) that facilitated stacking in the solid state, which was proposed to be a prerequisite for the formation of soft columnar mesophases, and assisted in decorrelating the neighboring columnar stacks at higher temperatures to form the plastic phases.(70,71)

Compound **5-Cp(CN)$_5$-1** also exhibits solid-state molecular stacking, albeit only with regard to the planar anions. In contrast, the nonmesomorphic iodide salt **5-I-1** lacks a columnar stacking motif in the crystalline solid state (Figures 5 and S25–S27).(72) Collectively, these results identify $[Cp(CN)_5]^-$ as a stable and compact mesogenic building block as it appears to maintain a so-called "charge-segregated" stacking, even at elevated temperatures.(73) Although the corresponding $[(C_1)_5im]^+$ cations are not mesogenic, they effectively function as "softening" structural constituents whose distribution around the stacks of $[Cp(CN)_5]^-$ anions becomes uniform above a certain temperature, thereby losing their correlated in-plane orientations.(74) Although it is not yet clear whether the fast rotations of the methyl substituents are important to facilitate the overall motions of the cations, the rotational motions of the peripheral $[BF_4]^-$ anions were proposed to play an active role in the decorrelation of neighboring cationic columns found in the LC mesophases adopted by 2,4,6-tris[3,4-bis(alkyloxy)phenyl]pyrylium $[BF_4]^-$ salts bearing short alkyl chains.(75)

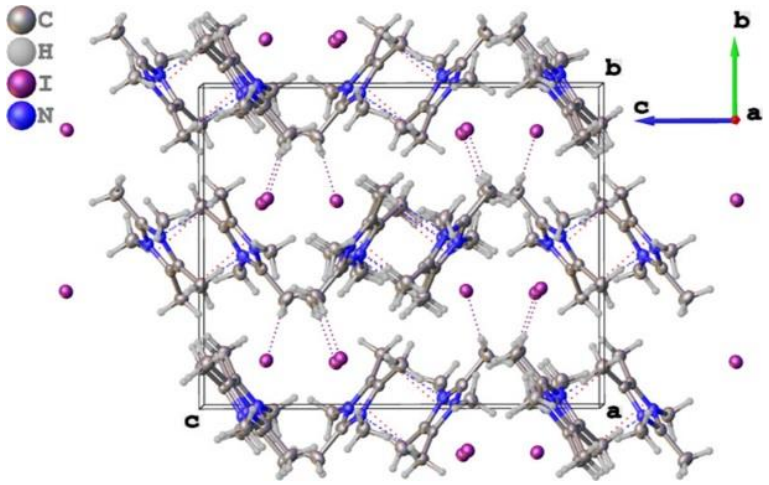

Figure 5. Packing in the crystal structure of **5-I-1**, showing the absence of a columnar stacking motif. The molecules are linked through nonclassical C–H···N (blue dotted lines) and C–H···I (purple dotted lines) hydrogen bonds as well as hydrogen-to-ring ("C–H···π") interactions (red dotted lines). See also Section S6.1 in the Supporting Information.

Finally, the thermodynamic parameters of the aforementioned phase transitions were evaluated. The entropy of fusion, ΔS_{fus}, that was measured for **5-Cp(CN)$_5$-1** (23 J K^{-1} mol^{-1}, see Table 1) is significantly lower than the upper limit of 40 J K^{-1} mol^{-1} for OIPCs that was proposed by MacFarlane and co-workers.(31,40) The measured ΔS_{fus} value even approaches Timmermans' original criterion of ΔS_{fus} < 20 J K^{-1} mol^{-1} for plastic crystal behavior.(76) Based on this criterion, the entropy data support the hypothesis that the M$_{hex}$ phase of **5-Cp(CN)$_5$-1** involves motions of the [(C$_1$)$_5$im]$^+$ cations as well as the [Cp(CN)$_5$]$^-$ anions.(31,40) The relatively small ΔS_{fus} values of compounds **5-Br-7** and **5-Cp(CN)$_5$-11** can be ascribed to incomplete crystallization during the DSC measurements.

2.3. Ionic Conductivity Displayed by Compound 5-Cp(CN)$_5$-1 and Its Mixtures with Na[Cp(CN)$_5$]

Because the M$_{hex}$ mesophase described above featured structural characteristics that were potentially conducive for anisotropic ion conduction, a series of ionic conductivity measurements were performed. The analyses were done upon cooling over a range of temperatures using the alternating current impedance method in conjunction with a sample cell equipped with comb-shaped gold electrodes.(77,78) The pure salt **5-Cp(CN)$_5$-1** was measured first and, as shown in Figure 6, an Arrhenius plot was constructed using the recorded data. The ionic conductivity in the M$_{hex}$ phase (σ = 2.6 to 3.0 × 10^{-5} S cm^{-1}) was determined to be comparable to that in the isotropic liquid phase. This indicates that the formation of a long-range, anisotropic 2D lattice in the former enables a mechanism of effective ion conduction that compensates for the higher viscosity of the mesophase. Evaluation of the data yielded an activation energy, E_a, of 19 kJ mol^{-1} for ion conduction in the M$_{hex}$ phase, which was approximately two times lower than the E_a value that was calculated for the isotropic liquid phase (∼42 kJ mol^{-1}). The results indicate a relatively low energy barrier to ion mobility in the M$_{hex}$ phase, in accordance with the finding that the constituent ions are not engaged in a long-range 3D lattice.

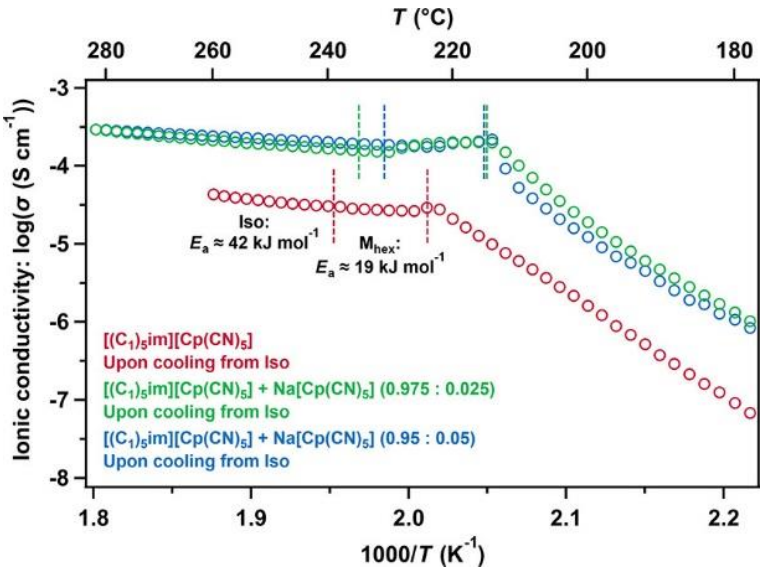

Figure 6. Dynamic ionic conductivity data (Arrhenius plots) recorded for **5-Cp(CN)$_5$-1** and for mixtures of **5-Cp(CN)$_5$-1** and Na[Cp(CN)$_5$] (molar ratios: 0.975:0.025 and 0.95:0.05). The thermal phase transitions are indicated by dashed lines.

To evaluate the effect of metal salt additives,(79−83) mixtures of **5-Cp(CN)$_5$-1** and Na[Cp(CN)$_5$] were also measured. Na^+ salts with weakly coordinating heterocyclic anions have recently attracted interest for use in sodium-ion batteries,(84,85) but Na[Cp(CN)$_5$] has, to the best of our knowledge, not yet been studied for this purpose.(86) **5-Cp(CN)$_5$-1**/Na[Cp(CN)$_5$] mixtures with molar ratios of 0.975:0.025 and 0.95:0.05 were prepared by slowly evaporating acetonitrile solutions of the two components followed by heating the samples to their isotropic liquid states. Upon cooling, plastic mesophases formed without phase separation.(87) The textures that were observed by POM were similar to those displayed by pure **5-Cp(CN)$_5$-1** (Figure S7). Introducing the Na^+ salt caused slight decreases in the phase-transition onset temperatures (Figures 6 and S20). Relatively high ionic conductivities in the range of 1.5 to 2.0 × 10^{-4} and 1.8 to 2.1 × 10^{-4} S cm^{-1} were measured for the nonaligned mesophases adopted by **5-Cp(CN)$_5$-1**/Na[Cp(CN)$_5$] (0.975:0.025) and **5-Cp(CN)$_5$-1**/Na[Cp(CN)$_5$] (0.95:0.05), respectively. The substantial increase in ionic conductivity upon addition of the Na^+ salt, by a factor of 8, indicates that conductivity values in the mS cm^{-1} range may be realized along with potential utility as anisotropic electrolytes in sodium-ion batteries.

3. Conclusions

We report the synthesis of a series of pentaalkylimidazolium salts as well as studies of their thermal characteristics and supramolecular organization. None of the amphiphilic compounds with relatively long alkyl chains and Br^-, $[NO_3]^-$, or $[Cp(CN)_5]^-$ counterions appear to be LC, although they are all low-melting salts. The amphiphilic $[Cp(CN)_5]^-$ salts are ILs below room temperature. In contrast, $[(C_1)_5im][Cp(CN)_5]$ was found to self-organize into an anisotropic, plastic crystal mesophase upon heating. The phase features rotating columnar stacks of $[Cp(CN)_5]^-$ anions that are arranged in a 2D lattice and positioned within a “continuum” formed by molten $[(C_1)_5im]^+$ cations that play the role of disorderly components. This binary system represents an original type of OIPC phase, which holds potential for use in electrochemical applications that require anisotropic ion conduction. Indeed, preliminary data show that high ionic conductivities can be achieved in the OIPC phase, particularly

after doping with a constituent Na^+ salt. In a broader perspective, the discovery represents a new paradigm in the field of OIPCs and establishes new design parameters for preparing highly ion-conductive, anisotropic electrolytes with tunable thermal characteristics. The results pertain to various domains of materials science, ranging from ILs through ionic plastic crystals and liquid crystals to the self-assembly of matter.

Future efforts may explore a systematic structure–property relationship of the $[Cp(CN)_5]^-$ salts in order to identify the molecular requirements for the emergence of the OIPC mesophase. Various structural variations of the imidazolium motif, including changes leading to symmetry reduction, should be synthetically accessible, such as modifications of (i) the number and positions of methyl groups on the imidazolium rings (i.e., $[(H)_x(C_1)_{5-x}im]^+$, where x = 2–5) or (ii) the nature and disposition of substituents on the imidazolium cores (i.e., $[(R)_x(C_1)_{5-x}im]^+$, where x = 2–3, and R = −C≡N, −Cl, ..., or $[(R_1)_x(R_2)_{5-x}im]^+$, where x = 2–3). The former materials may find utility in OIPC applications that require anisotropic proton conductivity. The latter can be expected to exhibit tunable thermal phase characteristics and surface activities in a manner that depends on the packing complementarities between the $[Cp(CN)_5]^-$ anions and the modified imidazolium cations.

4. Methods

4.1. General Procedures Nuclear magnetic resonance (NMR) spectra were recorded at ambient temperature (22.0(±1.0) °C, unless stated otherwise) on a Bruker ARX-300 spectrometer (operating at 300 MHz for ^{1}H), a Bruker AV-300 spectrometer (operating at 300 MHz for ^{1}H), a Bruker AV-400 spectrometer (operating at 400 MHz for ^{1}H), or a Bruker AVANCE III HD spectrometer (operating at 400 MHz for ^{1}H). Fourier transform infrared (FT-IR) spectra were recorded in attenuated total reflectance (ATR) mode on an Agilent Cary 630 FT-IR spectrometer using a germanium crystal (Ge-ATR). High-resolution mass spectra (HRMS) were recorded in electrospray ionization (ESI) mode on a Bruker Daltonics MicroTof mass spectrometer, a Thermo Scientific LTQ Orbitrap XL mass spectrometer, or a Waters Xevo G2-XS QTof mass spectrometer. Elemental analyses (carbon, hydrogen, nitrogen, and sulfur) were performed using a Thermo Scientific Flash 2000 Organic Elemental Analyzer. Optical textures were observed using an Olympus BX53-P polarized-light optical microscope that was equipped with a rotatable graduated sample platform and an Instec HCS402 dual heater temperature stage. The latter was equipped with a precision XY positioner and coupled to an Instec LN_2-SYS liquid nitrogen cooling system and an Instec mK2000 programmable temperature controller. Images were recorded with a QImaging Retiga 2000R CCD camera that was coupled to the microscope via a C mount. DSC data were recorded under nitrogen (50 mL min^{-1}) on a TA Instruments DSC Q2000 module equipped with an RCS90 cooling system at a heating rate of 10 °C min^{-1} and a cooling rate of 5 °C min^{-1}. The quantity of sample analyzed was typically 4–5 mg. A small hole was pierced into the lid of the aluminum sample pans. TGA data were recorded under nitrogen (60 mL min^{-1}) on a TA Instruments TGA Q500 module at a heating rate of 5 °C min^{-1} and using a platinum sample pan. The quantity of sample analyzed was typically 5–8 mg. Simultaneous TGA–DSC measurements were performed using a TA Instruments SDT Q600 module at a heating rate of 10 °C min^{-1} and under nitrogen (100 mL min^{-1}). An alumina sample pan was used. The quantity of sample analyzed was approximately 6.5 mg. To determine the crystal structures of compounds **5-I-1** and **5-Cp(CN)$_5$-1**, X-ray intensity data were collected at 123 K on a Rigaku XtaLAB P200 diffractometer equipped with a Pilatus 200K detector, using ω scans and Cu Kα radiation (wavelength λ = 1.54187 Å). See Section S6 in the Supporting Information for further details. Most of the SWAXS patterns were obtained with a transmission Guinier-like geometry. A linear focalized monochromatic Cu Kα1 beam (λ = 1.5405 Å) was obtained

using a sealed tube generator (600 W) equipped with a bent quartz monochromator. In all cases, the pristine powder was filled in Lindemann capillaries of 1 mm diameter and 10 µm wall thickness or in homemade sealed cells of 1 mm path length and equipped with 11 µm-thick aluminum windows. The diffraction patterns were recorded with a curved Inel CPS120 counter gas-filled detector linked to a data acquisition computer (periodicities up to 90 Å) and on image plates scanned by Amersham Typhoon IP with 25 µm resolution (periodicities up to 120 Å). The sample temperature could be varied between 20 and 200 °C with a precision of ±0.01 °C, and exposure times varied from 1 to 5 h. Synchrotron-based X-ray scattering measurements of the mesophase adopted by compound **5-Cp(CN)$_5$-1** were performed at the PLS-II 6D UNIST-PAL Beamline of the Pohang Accelerator Laboratory (PAL), Pohang, Republic of Korea. The X-rays coming from the bending magnet were monochromated using Si(111) double crystals and focused at the detector position by the combination of a second, sagittal-type monochromator crystal and a toroidal mirror system. The diffraction patterns were recorded by a Rayonix MX225-HS 2D CCD detector (225 × 225 mm^2 square active area, full resolution 5760 × 5760 pixels) with 2 × 2 binning. The peak positions in the one-dimensional intensity profiles, which were obtained from azimuthal averaging of the 2D patterns, were used for phase-type assignments. SWAXS patterns were recorded using 12.3984 keV X-ray radiation (wavelength λ = 1.00 Å) and a sample-to-detector distance of ca. 436 mm. Diffraction angles were calibrated using a lanthanum hexaboride (LaB_6) standard (NIST SRM 660c). Samples were contained in a borosilicate glass (glass #50) capillary with an outer diameter of 0.8 mm and a wall thickness of 10 µm and were irradiated for 5–10 s per measurement, depending on the saturation level of the detector. The capillaries were inserted into a custom-made brass holder that was placed into a Linkam TS1500V temperature stage to achieve temperature control. The samples were allowed to equilibrate at each temperature before starting a measurement. Dynamic ionic conductivity data were recorded with a Solartron (Schlumberger) SI 1260 impedance/gain-phase analyzer at a cooling rate of 2 °C min^{-1}, using a frequency range of 100 Hz to 20 MHz and a voltage of 0.6 V. The temperature was controlled using a Mettler-Toledo HS82 dual heater temperature stage that was coupled to a Mettler-Toledo HS1 programmable temperature controller. A glass sample cell with comb-shaped gold electrodes with thicknesses of 0.8 µm and spacings of 300 µm was used for all the measurements. The cell constant was determined using an aqueous KCl solution (0.01 M). Mixtures of **5-Cp(CN)$_5$-1** and Na[Cp(CN)$_5$] were prepared by slowly evaporating acetonitrile solutions of the two components followed by heating the samples to their isotropic liquid states.

4.2. Synthetic Procedures The reactions described below were performed in flame-dried or oven-dried glassware under an atmosphere of argon, unless specified otherwise. The given reaction temperatures correspond to the temperatures of the preheated oil baths that surrounded the reaction vessels. Unless specified otherwise, all reagents were purchased from commercial sources (Sigma-Aldrich, Alfa Aesar, Acros Organics, TCI Europe, and TCI Japan) and used without further purification. Anhydrous tetrahydrofuran (THF) was obtained by distillation in a continuous still under an atmosphere of argon over Na/benzophenone as the drying agent. The other anhydrous solvents were purchased from Carl Roth or Sigma-Aldrich and stored over molecular sieves under an atmosphere of argon. Anhydrous triethylamine was purchased from Sigma-Aldrich, distilled, and stored under an atmosphere of argon. The solvents that were used for column chromatography were of technical grade and were flash-distilled prior to use. During the syntheses of the precursors and the halide salts, reaction progress was monitored by thin-layer chromatography (TLC) on precoated, aluminum-backed plates (Merck Kieselgel 60 F_{254}). TLC spots were visualized by irradiation with a UV lamp and by immersion into a $KMnO_4$ stain. Purification by flash column chromatography was conducted using silica gel (60 Å, 35–70 µm, Kieselgel, Acros) with a head pressure of argon (0.1–0.3 atm).

*4.2.1. General Method for the Synthesis of Imidazole Precursors **4-n** (n = 7, 11, and 15)* 1,2-Diketone **3-*n*** (1 equiv), aldehyde **1-*n*** (1.2 equiv), and NH_4OAc (2.4 equiv) were dissolved in dry ethanol ([1,2-diketone] = 0.5 M) in a flame-dried Schlenk pressure tube, after which three drops of HOAc were added. The reaction mixture was stirred for 18 h at 110 °C under an atmosphere of argon. After cooling to room temperature (r.t.), the mixture was quenched with a saturated aqueous solution of $NaHCO_3$ and extracted with dichloromethane (3 × 30 mL per mmol). The combined organic layers were dried over anhydrous $MgSO_4$. After filtration, the solvent was removed under reduced pressure. The residue was purified by flash column chromatography (eluent: dichloromethane/methanol 100:0 → 93:7 v/v). See Section S1.2.1 in the Supporting Information for further details and analytical data.

*4.2.2. Synthesis of **5-I-1*** Compound **5-I-1** was synthesized by slowly adding iodomethane (80.32 mmol, 5.0 mL) to a stirred solution of 1,2,4,5-tetramethyl-1*H*-imidazole (40.27 mmol, 5.00 g) in 15 mL of dry acetonitrile in an oven-dried Schlenk pressure tube. The reaction mixture was covered from light and stirred for 18 h at 80 °C under an atmosphere of nitrogen. The solvent and excess of iodomethane were removed under reduced pressure. The crude product was washed with diethyl ether (3 × 40 mL) and recrystallized from acetone. Drying under reduced pressure at 50 °C afforded the desired product as a white powder. Yield: 95% (10.16 g). δ_H (400 MHz, CD_2Cl_2): 2.24 (s, 6H, (imidazolium C-4/C-5)−CH_3), 2.74 (s, 3H, (imidazolium C-2)−CH_3), 3.70 (s, 6H, N–CH_3). δ_C (101 MHz, $CDCl_3$): 9.1, 12.7, 33.2, 125.7, 142.8. IR (Ge-ATR): see Section S1.2.7 in the Supporting Information. HRMS (ESI, CH_2Cl_2, *m*/*z*): calcd for $[C_8H_{15}N_2]^+$ ([M – I^-]$^+$), 139.1230; found, 139.1233. Calcd for $C_8H_{15}IN_2$ (266.13): C, 36.11; H, 5.68; N, 10.53. Found: C, 36.00; H, 5.70; N, 10.86.

*4.2.3. General Method for the Synthesis of **5-Br-n** (n = 7, 11, 15)* The appropriate 2,4,5-trialkyl-1*H*-imidazole **4-*n*** (1 equiv), the appropriate 1-bromoalkane $C_nH_{2n+1}Br$ (15 equiv), and K_2CO_3 (2 equiv) were dissolved in dry THF ([2,4,5-trialkyl-1*H*-imidazole] = 0.3 M) in a flame-dried Schlenk pressure tube. The reaction mixture was stirred for 3 days at 80 °C under an atmosphere of argon. After cooling to r.t., the mixture was diluted with water. The resulting biphasic system was extracted with dichloromethane (3 × 20 mL per mmol). The combined organic layers were dried over anhydrous $MgSO_4$. After filtration, the solvent was removed under reduced pressure. The residue was purified by flash column chromatography (eluent: dichloromethane/methanol 100:0 → 93:7 v/v). To increase the isolated yield of pure product, the column fractions that contained a mixture of 1,2,4,5-tetraalkyl-1*H*-imidazole and 1,2,3,4,5-pentaalkyl-1*H*-imidazol-3-ium bromide were concentrated and resubjected to the aforementioned reaction conditions. See Section S1.2.2 in the Supporting Information for further details and analytical data.

*4.2.4. Synthesis of **5-NO₃-1*** The following steps were performed in the dark. A solution of compound **5-I-1** (3.86 mmol, 1.0279 g) in 10 mL of water was slowly added to a solution of silver nitrate (3.86 mmol, 0.6561 g) in 15 mL of water under stirring. The reaction mixture was stirred for 1.5 h at r.t. Insoluble products were filtered using a paper filter. The filtrate was concentrated under reduced pressure at 40 °C. The residue was redissolved in 20 mL of ethanol, and the solution was filtered using a PTFE syringe filter (0.1 µm pore size). After removing the solvent under reduced pressure at 40 °C, the residue was redissolved in 10 mL of dichloromethane and the solution was kept in a freezer overnight. Although visually there were no signs of precipitation, the solution was filtered using a PTFE syringe filter (0.1 µm pore size). Finally, the solution was concentrated and dried under reduced pressure at 60 °C to afford the desired product as a white powder. Small amounts of the product were dissolved in water and tested with NaBr or $AgNO_3$; the lack of a precipitate indicated that $AgNO_3$ and the iodide salt had been successfully removed. Yield: 95% (0.737 g). δ_H (400 MHz, DMSO-d_6): 2.21 (s, 6H, (imidazolium C-4/C-5)−CH_3), 2.57 (s, 3H, (imidazolium C-2)−CH_3), 3.61 (s, 6H, N–CH_3). δ_C (101 MHz, DMSO-d_6): 7.9, 9.6, 31.5, 124.9, 142.6. IR (Ge-ATR): see Section S1.2.7. HRMS (ESI, CH_3OH, *m*/*z*): calcd for $[C_8H_{15}N_2]^+$ ([M –

$[NO_3]^-]^+$), 139.1230; found, 139.1228. Calcd for $C_8H_{15}N_3O_3 \cdot 0.25H_2O$ (205.73): C, 47.75; H, 7.51; N, 20.88 (we note that, upon standing open to air, the compound rapidly absorbed additional water). Found: C, 47.42; H, 7.62; N, 20.45.

4.2.5. General Method for the Synthesis of ***5-NO₃-n*** *(n = 7, 11, 15)* The following steps were performed in the dark. A solution of the appropriate bromide salt **5-Br-*n*** (1 equiv) in ethanol ([**5-Br-*n***] = 0.04 M) was slowly added to a solution of silver nitrate (1.1 equiv) in ethanol ($[AgNO_3]$ = 0.1 M) under stirring. The reaction mixture was stirred for 15 h at r.t. Subsequently, 6 mL of dichloromethane was added. Insoluble products were filtered using a paper filter. The filtrate was concentrated under reduced pressure at 40 °C. The residue was redissolved in 20 mL of dichloromethane and washed two times with 5 mL of water. The organic layer was dried over anhydrous $MgSO_4$. After filtration, the solvent of the filtrate was removed under reduced pressure. See Section S1.2.3 in the Supporting Information for further details and analytical data.

4.2.6. Synthesis of ***5-Cp(CN)₅-1*** Under stirring, a solution of compound **5-I-1** (0.353 mmol, 0.0940 g) in 3 mL of water was slowly added to a solution of sodium pentacyanocyclopentadienide(57) (0.316 mmol, 0.0674 g) in 2 mL of water. The reaction mixture was stirred for 1 h at r.t. The off-white precipitate formed was filtered, washed with copious amounts of water, and then dried under reduced pressure at 50 °C for 48 h. Yield: 77% (0.080 g). δ_H (400 MHz, DMSO-d_6): 2.20 (s, 6H, (imidazolium C-4/C-5)−CH_3), 2.56 (s, 3H, (imidazolium C-2)−CH_3), 3.61 (s, 6H, N–CH_3). δ_C (101 MHz, DMSO-d_6): 8.0, 9.7, 31.6, 101.7 (−**C**≡N in $[Cp(CN)_5]^-$), 113.0 (C_{ring} in $[Cp(CN)_5]^-$), 125.0, 142.6. IR (Ge-ATR): see Section S1.2.7. HRMS (ESI, DMSO, *m*/*z*): calcd for $[C_8H_{15}N_2]^+$ ($[M - [Cp(CN)_5]^-]^+$), 139.1230; found, 139.1226. Calcd for $C_{18}H_{15}N_7$ (329.36): C, 65.64; H, 4.59; N, 29.77. Found: C, 65.26; H, 4.54; N, 29.40.

4.2.7. General Method for the Synthesis of ***5-Cp(CN)₅-n*** *(n = 7, 11, 15)* Under stirring, a solution of the appropriate bromide salt **5-Br-*n*** (1 equiv) in dry acetonitrile ([**5-Br-*n***] = 0.03 M) was slowly added to a solution of sodium pentacyanocyclopentadienide(57) (1 equiv) in dry acetonitrile ($[Na[Cp(CN)_5]]$ = 0.07 M). The reaction mixture was stirred for 1 h at r.t. (in the case of **5-Cp(CN)₅-7** and **5-Cp(CN)₅-11**) or at 65–70 °C (in the case of **5-Cp(CN)₅-15**). Subsequently, 30 mL of dichloromethane was added and the mixture was washed with 10 mL of water. The organic layer was separated and concentrated under reduced pressure at 40 °C. The residue was further dried overnight under reduced pressure at 40 °C, after which it was redissolved in 2.5 mL of dichloromethane. The solution was kept in a freezer overnight. Although visually there were no signs of precipitation, the solution was filtered using a PTFE syringe filter (0.1 μm pore size). Finally, the solution was concentrated and dried under reduced pressure at 50 °C. See Section S1.2.4 in the Supporting Information for further details and analytical data.

Supporting Information

The Supporting Information is available free of charge at https://pubs-acs-org.scd-rproxy.u-strasbg.fr/doi/10.1021/acs.chemmater.9b02338.

Methods, experimental details, and analytical data; POM, DSC, TGA, TGA–DSC, single-crystal XRD, and SWAXS data; and supplementary notes (PDF)

CIF files and CheckCIF reports of the crystal structures of compounds **5-I-1** and **5-Cp(CN)₅-1** (ZIP)

Author Contributions

K.G. and L.R. contributed equally to this work. All authors have given approval to the final version of the manuscript.

Notes

The authors declare no competing financial interest.

Acknowledgments

K.G., G.A., and C.W.B. were supported in part by the Institute for Basic Science (IBS-R019-D1). C.W.B. also acknowledges the BK21 Plus Program funded by the Ministry of Education and the National Research Foundation of Korea. L.R. and F.G. gratefully acknowledge the Deutsche Forschungsgemeinschaft (SFB 858). B.H. and B.D. thank the CNRS and the University of Strasbourg for support. K.G. and T.I. thank the Institute of Global Innovation Research at Tokyo University of Agriculture and Technology for financial support. The authors are grateful to Geonhui Park for synthesizing **5-I-1** and for recording the high-resolution mass spectrometric data. The authors thank Seong-Hun Lee for his assistance with the synchrotron SWAXS measurements. The experiments at the PLS-II 6D UNIST-PAL Synchrotron Beamline were supported in part by the Korean Ministry of Science and ICT (MSIT), Pohang University of Science and Technology (POSTECH), and the UNIST Central Research Facilities (UCRF).

References

1. *Ionic Liquids in Synthesis*; Wasserscheid, P., Welton, T., Eds.; Wiley-VCH: Weinheim, 2003. Google Scholar
2. Endres, F.; Zein El Abedin, S. Air and Water Stable Ionic Liquids in Physical Chemistry. *Phys. Chem. Chem. Phys.* **2006**, *8*, 2101– 2116, DOI: 10.1039/b600519p [Crossref], [PubMed], [CAS], Google Scholar
3. Hallett, J. P.; Welton, T. Room-Temperature Ionic Liquids: Solvents for Synthesis and Catalysis. 2. *Chem. Rev.* **2011**, *111*, 3508– 3576, DOI: 10.1021/cr1003248 [ACS Full Text], [CAS], Google Scholar
4. Goossens, K.; Lava, K.; Bielawski, C. W.; Binnemans, K. Ionic Liquid Crystals: Versatile Materials. *Chem. Rev.* **2016**, *116*, 4643– 4807, DOI: 10.1021/cr400334b [ACS Full Text], [CAS], Google Scholar
5. Mansueto, M.; Laschat, S. Ionic Liquid Crystals. In *Handbook of Liquid Crystals*; 2nd ed.; Goodby, J. W., Collings, P. J., Kato, T., Tschierske, C., Gleeson, H., Raynes, P., Eds.; Wiley-VCH: Weinheim, 2014; Volume 6: Nanostructured and Amphiphilic Liquid Crystals, pp 231– 280.[Crossref], Google Scholar
6. Fernandez, A. A.; Kouwer, P. H. J. Key Developments in Ionic Liquid Crystals. *Int. J. Mol. Sci.* **2016**, *17*, 731, DOI: 10.3390/ijms17050731 [Crossref], [CAS], Google Scholar
7. Kato, T.; Yoshio, M.; Ichikawa, T.; Soberats, B.; Ohno, H.; Funahashi, M. Transport of Ions and Electrons in Nanostructured Liquid Crystals. *Nat. Rev. Mater.* **2017**, *2*, 17001, DOI: 10.1038/natrevmats.2017.1 [Crossref], Google Scholar

8. Galiński, M.; Lewandowski, A.; Stepniak, I. Ionic Liquids As Electrolytes. *Electrochim. Acta* **2006**, *51*, 5567– 5580, DOI: 10.1016/j.electacta.2006.03.016 [Crossref], [CAS], Google Scholar
9. Armand, M.; Endres, F.; MacFarlane, D. R.; Ohno, H.; Scrosati, B. Ionic-Liquid Materials for the Electrochemical Challenges of the Future. *Nat. Mater.* **2009**, *8*, 621– 629, DOI: 10.1038/nmat2448 [Crossref], [PubMed], [CAS], Google Scholar
10. MacFarlane, D. R.; Tachikawa, N.; Forsyth, M.; Pringle, J. M.; Howlett, P. C.; Elliott, G. D.; Davis, J. H.; Watanabe, M.; Simon, P.; Angell, C. A. Energy Applications of Ionic Liquids. *Energy Environ. Sci.* **2014**, *7*, 232– 250, DOI: 10.1039/c3ee42099j [Crossref], [CAS], Google Scholar
11. Watanabe, M.; Thomas, M. L.; Zhang, S.; Ueno, K.; Yasuda, T.; Dokko, K. Application of Ionic Liquids to Energy Storage and Conversion Materials and Devices. *Chem. Rev.* **2017**, *117*, 7190– 7239, DOI: 10.1021/acs.chemrev.6b00504 [ACS Full Text], [CAS], Google Scholar
12. McEwen, A. B.; Ngo, H. L.; LeCompte, K.; Goldman, J. L. Electrochemical Properties of Imidazolium Salt Electrolytes for Electrochemical Capacitor Applications. *J. Electrochem. Soc.* **1999**, *146*, 1687– 1695, DOI: 10.1149/1.1391827 [Crossref], [CAS], Google Scholar
13. Wu, J.; Lan, Z.; Lin, J.; Huang, M.; Huang, Y.; Fan, L.; Luo, G. Electrolytes in Dye-Sensitized Solar Cells. *Chem. Rev.* **2015**, *115*, 2136– 2173, DOI: 10.1021/cr400675m [ACS Full Text], [CAS], Google Scholar
14. Yoshio, M.; Kagata, T.; Hoshino, K.; Mukai, T.; Ohno, H.; Kato, T. One-Dimensional Ion-Conductive Polymer Films: Alignment and Fixation of Ionic Channels Formed by Self-Organization of Polymerizable Columnar Liquid Crystals. *J. Am. Chem. Soc.* **2006**, *128*, 5570– 5577, DOI: 10.1021/ja0606935 [ACS Full Text], [CAS], Google Scholar
15. Yamanaka, N.; Kawano, R.; Kubo, W.; Masaki, N.; Kitamura, T.; Wada, Y.; Watanabe, M.; Yanagida, S. Dye-Sensitized TiO_2 Solar Cells Using Imidazolium-Type Ionic Liquid Crystal Systems As Effective Electrolytes. *J. Phys. Chem. B* **2007**, *111*, 4763– 4769, DOI: 10.1021/jp0671446 [ACS Full Text], [CAS], Google Scholar
16. Lee, S.-g. Functionalized Imidazolium Salts for Task-Specific Ionic Liquids and Their Applications. *Chem. Commun.* **2006**, 1049– 1063, DOI: 10.1039/b514140k [Crossref], [PubMed], [CAS], Google Scholar
17. Douce, L.; Suisse, J.-M.; Guillon, D.; Taubert, A. Imidazolium-Based Liquid Crystals: A Modular Platform for Versatile New Materials With Finely Tuneable Properties and Behaviour. *Liq. Cryst.* **2011**, *38*, 1653– 1661, DOI: 10.1080/02678292.2011.610474 [Crossref], [CAS], Google Scholar
18. Scalfani, V. F.; Al Alshaikh, A.; Bara, J. E. Analysis of the Frequency and Diversity of 1,3-Dialkylimidazolium Ionic Liquids Appearing in the Literature. *Ind. Eng. Chem. Res.* **2018**, *57*, 15971– 15981, DOI: 10.1021/acs.iecr.8b02573 [ACS Full Text], [CAS], Google Scholar
19. Bara, J. E.; Shannon, M. S. Beyond 1,3-Difunctionalized Imidazolium Cations. *Nanomater. Energy* **2012**, *1*, 237– 242, DOI: 10.1680/nme.12.00011 [Crossref], [CAS], Google Scholar
20. An archetypical example is the bis(trifluoromethylsulfonyl)imide (i.e., $[N(SO_2CF_3)_2]^-$ or $[NTf_2]^-$) anion; see, for example:Bonhôte, P.; Dias, A.-P.; Papageorgiou, N.; Kalyanasundaram, K.; Grätzel, M. Hydrophobic, Highly Conductive Ambient-Temperature Molten Salts. *Inorg. Chem.* **1996**, *35*, 1168– 1178, DOI: 10.1021/ic951325x [ACS Full Text], [CAS], Google Scholar
21. MacFarlane, D. R.; Golding, J.; Forsyth, S.; Forsyth, M.; Deacon, G. B. Low Viscosity Ionic Liquids Based on Organic Salts of the Dicyanamide Anion. *Chem. Commun.* **2001**, 1430– 1431, DOI: 10.1039/b103064g [Crossref], [CAS], Google Scholar
22. MacFarlane, D. R.; Forsyth, S. A.; Golding, J.; Deacon, G. B. Ionic Liquids Based on Imidazolium, Ammonium and Pyrrolidinium Salts of the Dicyanamide Anion. *Green Chem.* **2002**, *4*, 444– 448, DOI: 10.1039/b205641k [Crossref], [CAS], Google Scholar
23. Park, G.; Goossens, K.; Shin, T. J.; Bielawski, C. W. Dicyanamide Salts That Adopt Smectic, Columnar, or Bicontinuous Cubic Liquid-Crystalline Mesophases. *Chem.—Eur. J.* **2018**, *24*, 6399– 6411, DOI: 10.1002/chem.201705794 [Crossref], [PubMed], [CAS], Google Scholar

24. Pringle, J. M.; Howlett, P. C.; MacFarlane, D. R.; Forsyth, M. Organic Ionic Plastic Crystals: Recent Advances. *J. Mater. Chem.* **2010**, *20*, 2056– 2062, DOI: 10.1039/b920406g [Crossref], [CAS], Google Scholar
25. Pringle, J. M. Recent Progress in the Development and Use of Organic Ionic Plastic Crystal Electrolytes. *Phys. Chem. Chem. Phys.* **2013**, *15*, 1339– 1351, DOI: 10.1039/c2cp43267f [Crossref], [PubMed], [CAS], Google Scholar
26. MacFarlane, D. R.; Forsyth, M.; Howlett, P. C.; Kar, M.; Passerini, S.; Pringle, J. M.; Ohno, H.; Watanabe, M.; Yan, F.; Zheng, W.Ionic Liquids and Their Solid-State Analogues As Materials for Energy Generation and Storage. *Nat. Rev. Mater.* **2016**, *1*, 15005, DOI: 10.1038/natrevmats.2015.5 [Crossref], [PubMed], [CAS], Google Scholar
27. Rana, U. A.; Forsyth, M.; MacFarlane, D. R.; Pringle, J. M. Toward Protic Ionic Liquid and Organic Ionic Plastic Crystal Electrolytes for Fuel Cells. *Electrochim. Acta* **2012**, *84*, 213– 222, DOI: 10.1016/j.electacta.2012.03.058 [Crossref], [CAS], Google Scholar
28. Basile, A.; Hilder, M.; Makhlooghiazad, F.; Pozo-Gonzalo, C.; MacFarlane, D. R.; Howlett, P. C.; Forsyth, M. Ionic Liquids and Organic Ionic Plastic Crystals: Advanced Electrolytes for Safer High Performance Sodium Energy Storage Technologies. *Adv. Energy Mater.* **2018**, *8*, 1703491, DOI: 10.1002/aenm.201703491 [Crossref], Google Scholar
29. Jin, L.; Nairn, K. M.; Forsyth, C. M.; Seeber, A. J.; MacFarlane, D. R.; Howlett, P. C.; Forsyth, M.; Pringle, J. M. Structure and Transport Properties of a Plastic Crystal Ion Conductor: Diethyl(Methyl)(Isobutyl)Phosphonium Hexafluorophosphate. *J. Am. Chem. Soc.* **2012**, *134*, 9688– 9697, DOI: 10.1021/ja301175v [ACS Full Text], [CAS], Google Scholar
30. Luo, J.; Jensen, A. H.; Brooks, N. R.; Sniekers, J.; Knipper, M.; Aili, D.; Li, Q.; Vanroy, B.; Wübbenhorst, M.; Yan, F.1,2,4-Triazolium Perfluorobutanesulfonate As an Archetypal Pure Protic Organic Ionic Plastic Crystal Electrolyte for All-Solid-State Fuel Cells. *Energy Environ. Sci.* **2015**, *8*, 1276– 1291, DOI: 10.1039/c4ee02280g [Crossref], [CAS], Google Sch
31. MacFarlane, D. R.; Meakin, P.; Sun, J.; Amini, N.; Forsyth, M. Pyrrolidinium Imides: A New Family of Molten Salts and Conductive Plastic Crystal Phases. *J. Phys. Chem. B* **1999**, *103*, 4164– 4170, DOI: 10.1021/jp984145s [ACS Full Text], [CAS], Google Scholar
32. Jin, L.; Nairn, K. M.; Ling, C. D.; Zhu, H.; O'Dell, L. A.; Li, J.; Chen, F.; Pavan, A. F.; Madsen, L. A.; Howlett, P. C.Conformational Dynamics in an Organic Ionic Plastic Crystal. *J. Phys. Chem. B* **2017**, *121*, 5439– 5446, DOI: 10.1021/acs.jpcb.7b02780 [ACS Full Text], [CAS], Google Scholar
33. Lee, M.; Choi, U. H.; Wi, S.; Slebodnick, C.; Colby, R. H.; Gibson, H. W. 1,2-Bis[N-(N'-alkylimidazolium)]ethane salts: a new class of organic ionic plastic crystals. *J. Mater. Chem.* **2011**, *21*, 12280– 12287, DOI: 10.1039/c1jm10995b [Crossref], [CAS], Google Scholar
34. Kidd, B. E.; Lingwood, M. D.; Lee, M.; Gibson, H. W.; Madsen, L. A. Cation and Anion Transport in a Dicationic Imidazolium-Based Plastic Crystal Ion Conductor. *J. Phys. Chem. B* **2014**, *118*, 2176– 2185, DOI: 10.1021/jp4084629 [ACS Full Text], [CAS], Google Scholar
35. Lee, M.; Lee, Y.-H.; Park, J. H.; Choi, U. H. Bis-Imidazolium Iodide Organic Ionic Plastic Crystals and Their Applications to Solid State Dye-Sensitized Solar Cells. *Org. Electron.* **2017**, *48*, 241– 247, DOI: 10.1016/j.orgel.2017.06.004 [Crossref], [CAS], Google Scholar
36. Yoshizawa-Fujita, M.; Fujita, K.; Forsyth, M.; MacFarlane, D. R. A New Class of Proton-Conducting Ionic Plastic Crystals Based on Organic Cations and Dihydrogen Phosphate. *Electrochem. Commun.* **2007**, *9*, 1202– 1205, DOI: 10.1016/j.elecom.2007.01.024 [Crossref], [CAS], Google Scholar
37. Luo, J.; Conrad, O.; Vankelecom, I. F. J. Imidazolium Methanesulfonate As a High Temperature Proton Conductor. *J. Mater. Chem. A* **2013**, *1*, 2238– 2247, DOI: 10.1039/c2ta00713d [Crossref], [CAS], Google Scholar
38. Chong, A. L.; Zhu, H.; Nairn, K. M.; Forsyth, M.; MacFarlane, D. R. Enhancing Solid-State Conductivity Through Acid or Base Doping of Protic Imidazolium and Imidazolinium Triflate Salts. *J. Phys. Chem. C* **2017**, *121*, 27849– 27859, DOI: 10.1021/acs.jpcc.7b10275 [ACS Full Text], [CAS], Google Scholar

39. Zhu, H.; Wang, X.; Vijayaraghava, R.; Zhou, Y.; MacFarlane, D. R.; Forsyth, M. Structure and Ion Dynamics in Imidazolium-Based Protic Organic Ionic Plastic Crystals. *J. Phys. Chem. Lett.* **2018**, *9*, 3904– 3909, DOI: 10.1021/acs.jpclett.8b01500 [ACS Full Text], [CAS], Google Scholar
40. MacFarlane, D. R.; Meakin, P.; Amini, N.; Forsyth, M. Structural Studies of Ambient Temperature Plastic Crystal Ion Conductors. *J. Phys.: Condens. Matter* **2001**, *13*, 8257– 8267, DOI: 10.1088/0953-8984/13/36/303 [Crossref], [CAS], Google Scholar
41. Fox, D. M.; Awad, W. H.; Gilman, J. W.; Maupin, P. H.; De Long, H. C.; Trulove, P. C. Flammability, Thermal Stability, and Phase Change Characteristics of Several Trialkylimidazolium Salts. *Green Chem.* **2003**, *5*, 724– 727, DOI: 10.1039/B308444B [Crossref], [CAS], Google Scholar
42. Mukai, T.; Yoshio, M.; Kato, T.; Yoshizawa-Fujita, M.; Ohno, H. Self-Organization of Protonated 2-Heptadecylimidazole As an Effective Ion Conductive Matrix. *Electrochemistry* **2005**, *73*, 623– 626, DOI: 10.5796/electrochemistry.73.623 [Crossref], [CAS], Google Scholar
43. Yoshio, M.; Ichikawa, T.; Shimura, H.; Kagata, T.; Hamasaki, A.; Mukai, T.; Ohno, H.; Kato, T. Columnar Liquid-Crystalline Imidazolium Salts. Effects of Anions and Cations on Mesomorphic Properties and Ionic Conductivity. *Bull. Chem. Soc. Jpn.* **2007**, *80*, 1836– 1841, DOI: 10.1246/bcsj.80.1836 [Crossref], [CAS], Google Scholar
44. Kouwer, P. H. J.; Swager, T. M. Synthesis and Mesomorphic Properties of Rigid-Core Ionic Liquid Crystals. *J. Am. Chem. Soc.* **2007**, *129*, 14042– 14052, DOI: 10.1021/ja075651a [ACS Full Text], [CAS], Google Scholar
45. Endo, T.; Kato, T.; Nishikawa, K. Effects of Methylation at the 2 Position of the Cation Ring on Phase Behaviors and Conformational Structures of Imidazolium-Based Ionic Liquids. *J. Phys. Chem. B* **2010**, *114*, 9201– 9208, DOI: 10.1021/jp104123v [ACS Full Text], [CAS], Google Scholar
46. Goossens, K.; Wellens, S.; Van Hecke, K.; Van Meervelt, L.; Cardinaels, T.; Binnemans, K. T-Shaped Ionic Liquid Crystals Based on the Imidazolium Motif: Exploring Substitution of the C-2 Imidazolium Carbon Atom. *Chem.—Eur. J.* **2011**, *17*, 4291– 4306, DOI: 10.1002/chem.201001921 [Crossref], [PubMed], [CAS], Google Scholar
47. Nestor, S. T.; Heinrich, B.; Sykora, R. A.; Zhang, X.; McManus, G. J.; Douce, L.; Mirjafari, A. Methimazolium-Based Ionic Liquid Crystals: Emergence of Mesomorphic Properties Via a Sulfur Motif. *Tetrahedron* **2017**, *73*, 5456– 5460, DOI: 10.1016/j.tet.2017.07.056 [Crossref], [CAS], Google Scholar
48. $[(C_2)_5im][NO_3]$ was described in a patent application; see: Qiao, F.; Wang, S. Lithium ion battery electrolyte and lithium ion battery containing the same. CN102412418A, 2012.Google Scholar
49. Permethylated $[(C_1)_5im][X]$ salts are known but, to the best of our knowledge, none have been reported to be mesomorphic [see, for example: $X^- = [NTf_2]^-$ (T_m = 118 °C): Ngo, H. L.; McEwen, A. B. Pentamethyl Imidazolium Salts. *Electrochem. Soc. Proc.***1999,***98,* 683–692].
50. Richter, C.; Schaepe, K.; Glorius, F.; Ravoo, B. J. Tailor-Made N-Heterocyclic Carbenes for Nanoparticle Stabilization. *Chem. Commun.* **2014**, *50*, 3204– 3207, DOI: 10.1039/c4cc00654b [Crossref], [PubMed], [CAS], Google Scholar
51. Wang, D.; Richter, C.; Rühling, A.; Drücker, P.; Siegmund, D.; Metzler-Nolte, N.; Glorius, F.; Galla, H.-J. A Remarkably Simple Class of Imidazolium-Based Lipids and Their Biological Properties. *Chem.—Eur. J.* **2015**, *21*, 15123– 15126, DOI: 10.1002/chem.201502333 [Crossref], [PubMed], [CAS], Google Scholar
52. Wang, D.; Richter, C.; Rühling, A.; Hüwel, S.; Glorius, F.; Galla, H.-J. Anti-Tumor Activity and Cytotoxicity in Vitro of Novel 4,5-Dialkylimidazolium Surfactants. *Biochem. Biophys. Res. Commun.* **2015**, *467*, 1033– 1038, DOI: 10.1016/j.bbrc.2015.10.015 [Crossref], [PubMed], [CAS], Google Scholar
53. Rühling, A.; Wang, D.; Ernst, J. B.; Wulff, S.; Honeker, R.; Richter, C.; Ferry, A.; Galla, H.-J.; Glorius, F. Influence of the Headgroup of Azolium-Based Lipids on Their Biophysical Properties and Cytotoxicity. *Chem.—Eur. J.* **2017**, *23*, 5920– 5924, DOI: 10.1002/chem.201604182 [Crossref], [PubMed], [CAS], Google Scholar

54. Drücker, P.; Rühling, A.; Grill, D.; Wang, D.; Draeger, A.; Gerke, V.; Glorius, F.; Galla, H.-J. Imidazolium Salts Mimicking the Structure of Natural Lipids Exploit Remarkable Properties Forming Lamellar Phases and Giant Vesicles. *Langmuir* **2017**, *33*, 1333– 1342, DOI: 10.1021/acs.langmuir.6b03182 [ACS Full Text], [CAS], Google Scholar
55. Goossens, K.; Rakers, L.; Shin, T.; Honeker, R.; Bielawski, C. W.; Glorius, F. Substituted Azolium Disposition: Examining the Effects of Alkyl Placement on Thermal Properties. *Crystals* **2019**, *9*, 34, DOI: 10.3390/cryst9010034 [Crossref], [CAS], Google Scholar
56. Despite their lower reactivity, 1-bromoalkanes were used instead of 1-iodoalkanes to facilitate a comparison of the thermal characteristics of the resulting pentaalkylimidazolium bromide salts to those of imidazolium bromide derivatives with fewer alkyl chains. The latter have been more widely studied as compared to the iodide salts, in part due to the smaller size of the bromide anion as compared to iodide and due to the higher photostability of bromide salts.
57. Sakai, T.; Seo, S.; Matsuoka, J.; Mori, Y. Synthesis of Functionalized Tetracyanocyclopentadienides From Tetracyanothiophene and Sulfones. *J. Org. Chem.* **2013**, *78*, 10978– 10985, DOI: 10.1021/jo401946j [ACS Full Text], [CAS], Google Scholar
58. For comparison, long-chain-substituted 1-alkyl-3-methylimidazolium bromide ([$C_n$mim][Br]) and 1,3-dialkylimidazolium bromide ([$(C_n)_2$im][Br]) salts are typically stable monohydrates, even when exposed to ambient atmospheres. See, for example, refs 23 and 24 in the Supporting Information.
59. Such an arrangement was previously observed in the solid-state structure of the non-mesomorphic salt [tropylium][$Cp(CN)_5$], see ref (73).
60. Wöhrle, T.; Wurzbach, I.; Kirres, J.; Kostidou, A.; Kapernaum, N.; Litterscheidt, J.; Haenle, J. C.; Staffeld, P.; Baro, A.; Giesselmann, F.Discotic Liquid Crystals. *Chem. Rev.* **2016**, *116*, 1139– 1241, DOI: 10.1021/acs.chemrev.5b00190 [ACS Full Text], [CAS], Google Scholar
61. The mesomorphism of so-called “flying-seed-like” LCs, which also lack flexible chains, was proposed to originate from thermal fluctuations due to free rotation of the bulky substituents (thus creating “soft” parts) [see, for example: Ohta, K.; Shibuya, T.; Ando, M. Flying-seed-like liquid crystals. *J. Mater. Chem.***2006,***16,* 3635–3639].
62. Seeber, A. J.; Forsyth, M.; Forsyth, C. M.; Forsyth, S. A.; Annat, G.; MacFarlane, D. R. Conductivity, NMR and Crystallographic Study of N,N,N,N-Tetramethylammonium Dicyanamide Plastic Crystal Phases: an Archetypal Ambient Temperature Plastic Electrolyte Material. *Phys. Chem. Chem. Phys.* **2003**, *5*, 2692– 2698, DOI: 10.1039/b212743a [Crossref], [CAS], Google Scholar
63. Annat, G.; Adebahr, J.; McKinnon, I.; MacFarlane, D. R.; Forsyth, M. Plastic Crystal Behaviour in Tetraethylammonium Dicyanamide. *Solid State Ionics* **2007**, *178*, 1065– 1071, DOI: 10.1016/j.ssi.2007.04.015 [Crossref], [CAS], Google Scholar
64. Yoon, H.; Lane, G. H.; Shekibi, Y.; Howlett, P. C.; Forsyth, M.; Best, A. S.; MacFarlane, D. R. Lithium Electrochemistry and Cycling Behaviour of Ionic Liquids Using Cyano Based Anions. *Energy Environ. Sci.* **2013**, *6*, 979– 986, DOI: 10.1039/c3ee23753b [Crossref], [CAS], Google Scholar
65. Pringle, J. M.; Golding, J.; Forsyth, C. M.; Deacon, G. B.; Forsyth, M.; MacFarlane, D. R. Physical Trends and Structural Features in Organic Salts of the Thiocyanate Anion. *J. Mater. Chem.* **2002**, *12*, 3475– 3480, DOI: 10.1039/b208372h [Crossref], [CAS], Google Scholar
66. Adebahr, J.; Grimsley, M.; Rocher, N. M.; MacFarlane, D. R.; Forsyth, M. Rotational and Translational Mobility of a Highly Plastic Salt: Dimethylpyrrolidinium Thiocyanate. *Solid State Ionics* **2008**, *178*, 1798– 1803, DOI: 10.1016/j.ssi.2007.12.017 [Crossref], [CAS], Google Scholar
67. Golding, J.; Forsyth, S.; MacFarlane, D. R.; Forsyth, M.; Deacon, G. B. Methanesulfonate and *p*-Toluenesulfonate Salts of the N-Methyl-N-Alkylpyrrolidinium and Quaternary Ammonium Cations: Novel Low Cost Ionic Liquids. *Green Chem.* **2002**, *4*, 223– 229, DOI: 10.1039/b201063a [Crossref], [CAS], Google Scholar
68. Cahill, L. S.; Rana, U. A.; Forsyth, M.; Smith, M. E. Investigation of Proton Dynamics and the Proton Transport Pathway in Choline Dihydrogen Phosphate Using Solid-State NMR. *Phys. Chem. Chem. Phys.* **2010**, *12*, 5431– 5438, DOI: 10.1039/b916422g [Crossref], [PubMed], [CAS], Google Scholar

69. Sirota, E. B.; King, H. E.; Singer, D. M.; Shao, H. H. Rotator Phases of the Normal Alkanes - An X-Ray-Scattering Study. *J. Chem. Phys.* **1993**, *98*, 5809– 5824, DOI: 10.1063/1.464874 [Crossref], [CAS], Google Scholar
70. Barberá, J.; Rakitin, O. A.; Ros, M. B.; Torroba, T. Breaking the Mold of Discotic Liquid Crystals. *Angew. Chem., Int. Ed.* **1998**, *37*, 296– 299, DOI: 10.1002/(sici)1521-3773(19980216)37:3<296::aid-anie296>3.0.co;2-u [Crossref], [CAS], Google Scholar
71. Basurto, S.; García, S.; Neo, A. G.; Torroba, T.; Marcos, C. F.; Miguel, D.; Barberá, J.; Ros, M. B.; de la Fuente, M. R. Indene and Pseudoazulene Discotic Liquid Crystals: A Synthetic and Structural Study. *Chem.—Eur. J.* **2005**, *11*, 5362– 5376, DOI: 10.1002/chem.200500155 [Crossref], [PubMed], [CAS], Google Scholar
72. See also:Kuhn, N.; Henkel, G.; Kreutzberg, J. Synthese und Reaktionen von 1,2,4,5-Tetramethylimidazol; die Kristallstruktur von Pentamethylimidazolium-iodid/Synthesis and Reactions of 1,2,4,5-Tetramethylimidazole; the Crystal Structure of Pentamethylimidazolium Iodide. *Z. Naturforsch., B: J. Chem. Sci.* **1991**, *46b*, 1706– 1712, DOI: 10.1515/znb-1991-1221 [Crossref], Google Scholar
73. To the best of our knowledge, only Maeda and co-workers previously reported ILCs with $[Cp(CN)_5]^-$ anions and quaternary ammonium counterions with long alkyl chains, see:Bando, Y.; Sakurai, T.; Matsuda, W.; Seki, S.; Takaya, H.; Maeda, H. Ion-Pairing Assemblies Based on Pentacyano-Substituted Cyclopentadienide as a π-Electronic Anion. *Chem.—Eur. J.* **2016**, *22*, 7843– 7850, DOI: 10.1002/chem.201600686 [Crossref], [PubMed], [CAS], Google Scholar
74. We note that unsolvated $Na[Cp(CN)_5]$ also exhibits stacking of the $[Cp(CN)_5]^-$ anions in the solid state [Bacsa, J.; Less, R. J.; Skelton, H. E.; Soracevic, Z.; Steiner, A.; Wilson, T. C.; Wood, P. T.; Wright, D. S. Assembly of the First Fullerene-Type Metal–Organic Frameworks Using a Planar Five-Fold Coordination Node. *Angew. Chem., Int. Ed.***2011,***50,* 8279–8282], although the compound is a high-melting, non-mesomorphic solid (T_m = 483 °C, see Figure S24).
75. Veber, M.; Sotta, P.; Davidson, P.; Levelut, A. M.; Jallabert, C.; Strzelecka, H. Mesomorphic Properties of Short Chains Substituted Heteroaromatic Salts. *J. Phys.* **1990**, *51*, 1283– 1301, DOI: 10.1051/jphys:0199000510120128300 [Crossref], [CAS], Google Scholar
76. Timmermans, J. Plastic Crystals: A Historical Review. *J. Phys. Chem. Solids* **1961**, *18*, 1– 8, DOI: 10.1016/0022-3697(61)90076-2 [Crossref], [CAS], Google Scholar
77. Yoshio, M.; Mukai, T.; Kanie, K.; Yoshizawa, M.; Ohno, H.; Kato, T. Layered Ionic Liquids: Anisotropic Ion Conduction in New Self-Organized Liquid-Crystalline Materials. *Adv. Mater.* **2002**, *14*, 351– 354, DOI: 10.1002/1521-4095(20020304)14:5<351::aid-adma351>3.0.co;2-d [Crossref], [CAS], Google Scholar
78. Ichikawa, T.; Yoshio, M.; Hamasaki, A.; Taguchi, S.; Liu, F.; Zeng, X.-b.; Ungar, G.; Ohno, H.; Kato, T. Induction of Thermotropic Bicontinuous Cubic Phases in Liquid-Crystalline Ammonium and Phosphonium Salts. *J. Am. Chem. Soc.* **2012**, *134*, 2634– 2643, DOI: 10.1021/ja209010m [ACS Full Text], [CAS], Google Scholar
79. MacFarlane, D. R.; Huang, J.; Forsyth, M. Lithium-Doped Plastic Crystal Electrolytes Exhibiting Fast Ion Conduction for Secondary Batteries. *Nature* **1999**, *402*, 792– 794, DOI: 10.1038/45514 [Crossref], [CAS], Google Scholar
80. Forsyth, M.; Huang, J.; MacFarlane, D. R. Lithium Doped *N*-Methyl-*N*-Ethylpyrrolidinium Bis(Trifluoromethanesulfonyl)Amide Fast-Ion Conducting Plastic Crystals. *J. Mater. Chem.* **2000**, *10*, 2259– 2265, DOI: 10.1039/b003168m [Crossref], [CAS], Google Scholar
81. Jin, L.; Howlett, P.; Efthimiadis, J.; Kar, M.; MacFarlane, D.; Forsyth, M. Lithium Doped *N,N*-Dimethyl Pyrrolidinium Tetrafluoroborate Organic Ionic Plastic Crystal Electrolytes for Solid State Lithium Batteries. *J. Mater. Chem.* **2011**, *21*, 10171– 10178, DOI: 10.1039/c0jm04401f [Crossref], [CAS], Google Scholar
82. Moriya, M.; Kato, D.; Sakamoto, W.; Yogo, T. Plastic Crystalline Lithium Salt With Solid-State Ionic Conductivity and High Lithium Transport Number. *Chem. Commun.* **2011**, *47*, 6311– 6313, DOI: 10.1039/c1cc00070e [Crossref], [PubMed], [CAS], Google Scholar

83. Forsyth, M.; Chimdi, T.; Seeber, A.; Gunzelmann, D.; Howlett, P. C. Structure and Dynamics in an Organic Ionic Plastic Crystal, *N*-Ethyl-*N*-Methyl Pyrrolidinium Bis(Trifluoromethanesulfonyl) Amide, Mixed With a Sodium Salt. *J. Mater. Chem. A* **2014**, *2*, 3993– 4003, DOI: 10.1039/c3ta15153k [Crossref], [CAS], Google Scholar
84. Ponrouch, A.; Monti, D.; Boschin, A.; Steen, B.; Johansson, P.; Palacín, M. R. Non-Aqueous Electrolytes for Sodium-Ion Batteries. *J. Mater. Chem. A* **2015**, *3*, 22– 42, DOI: 10.1039/c4ta04428b [Crossref], [CAS], Google Scholar
85. Plewa-Marczewska, A.; Trzeciak, T.; Bitner, A.; Niedzicki, L.; Dranka, M.; Żukowska, G. Z.; Marcinek, M.; Wieczorek, W. New Tailored Sodium Salts for Battery Applications. *Chem. Mater.* **2014**, *26*, 4908– 4914, DOI: 10.1021/cm403349t [ACS Full Text], [CAS], Google Scholar
86. A theoretical study by Johansson and co-workers noted that Li^+ salts with fluorine-free $[N_5C_{2n}]^-$ anions ($0 \leq n \leq 5$) hold potential for use in lithium-ion batteries due to the low affinity between Li^+ and the anions as well as their high stability toward oxidation [see: Johansson, P.; Nilsson, H.; Jacobsson, P.; Armand, M. Novel Hückel stabilised azole ring-based lithium salts studied by *ab initio* Gaussian-3 theory. *Phys. Chem. Chem. Phys.***2004,***6,* 895–899]. To the best of our knowledge, $Li[Cp(CN)_5]$ has not yet been synthesized.
87. We note that no homogeneous mixtures were obtained for higher percentages of $Na[Cp(CN)_5]$, such as **5-Cp(CN)$_5$-1**/$Na[Cp(CN)_5]$ in a molar ratio of 0.9:0.1.